BIOCHEMISTRY
including biophysical chemistry & molecular biology

Article

pubs.acs.org/biochemistry

Collapse of a Long Axis: Single-Molecule Förster Resonance Energy Transfer and Serpin Equilibrium Unfolding

Lu Liu,[†,§] Michael Werner,[†,∥] and Anne Gershenson*[,‡]

[†]Department of Chemistry, Brandeis University, Waltham, Massachusetts 02453, United States

[‡]Department of Biochemistry and Molecular Biology, University of Massachusetts Amherst, Amherst, Massachusetts 01003, United States

Supporting Information

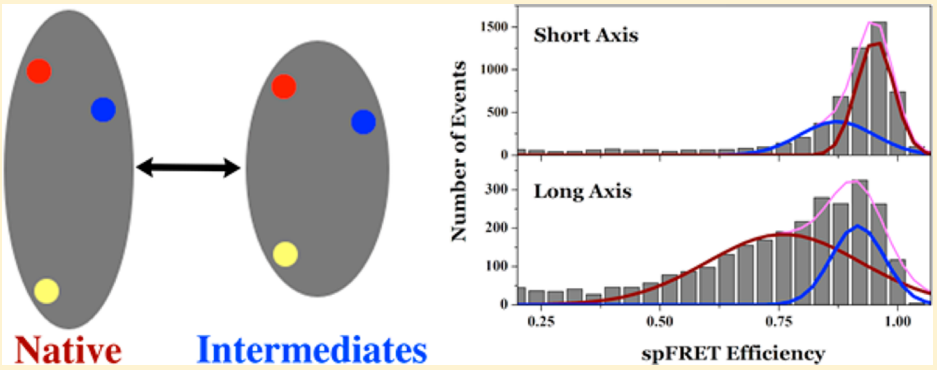

ABSTRACT: The energy required for mechanical inhibition of target proteases is stored in the native structure of inhibitory serpins and accessed by serpin structural remodeling. The overall serpin fold is ellipsoidal with one long and two short axes. Most of the structural remodeling required for function occurs along the long axis, while expansion of the short axes is associated with misfolded, inactive forms. This suggests that ellipticity, as typified by the long axis, may be important for both function and folding. Placement of donor and acceptor fluorophores approximately along the long axis or one of the short axes allows single-pair Förster resonance energy transfer (spFRET) to report on both unfolding transitions and the time-averaged shape of different conformations. Equilibrium unfolding and refolding studies of the well-characterized inhibitory serpin α_1-antitrypsin reveal that the long axis collapses in the folding intermediates while the monitored short axis expands. These energetically distinct intermediates are thus more spherical than the native state. Our spFRET studies agree with other equilibrium unfolding studies that found that the region around one of the β strands, s5A, which helps define the long axis and must move for functionally required loop insertion, unfolds at low denaturant concentrations. This supports a connection between functionally important structural lability and unfolding in the inhibitory serpins.

Inhibitory members of the serpin superfamily regulate serine and cysteine proteases required for critical physiological processes, including blood coagulation and inflammation.[1,2] Unlike canonical protease inhibitors that simply bind to the protease active site, inhibition by serpins requires mechanical deformation of the protease active site, mediated by extensive structural rearrangements and repacking of the serpin structure.[3,4] Serpin structural remodeling is triggered when a target protease cleaves the serpin's solvent-exposed reactive center loop (RCL) leading to insertion of the cleaved RCL into the center of β sheet A in the serpin and translocation of the covalently attached protease ~70 Å from one end of the serpin to the other (Figure 1).[1,3−6] Because the energy needed for serpin structural remodeling and the associated protease inhibition is stored in the strained, metastable structure of active inhibitory serpins,[7−9] inhibitory serpins must fold to a kinetically trapped, metastable conformation that is not the global energy minimum.

The ellipsoidal fold of active serpins is characterized by one long axis, ~70 Å in length for the canonical serpin, α_1-antitrypsin (α_1AT, also known as α_1-proteinase inhibitor), and two approximately equal short axes, ~45 Å each for α_1AT (Figure 1). This watermelon-shaped fold is composed of three β sheets, A−C, and nine α helices in two well-connected domains.[1,2] The watermelon shape is defined by the serpin long axis that is largely coincident with sheet A, the largest of the β sheets and the β sheet most directly involved in protease inhibition as well as other, nonproductive conformations. These lower-energy, nonfunctional conformations include the latent form in which the intact RCL inserts into β sheet A in the absence of cleavage[10,11] and polymeric forms involving

Received: December 4, 2013
Revised: March 17, 2014
Published: April 22, 2014

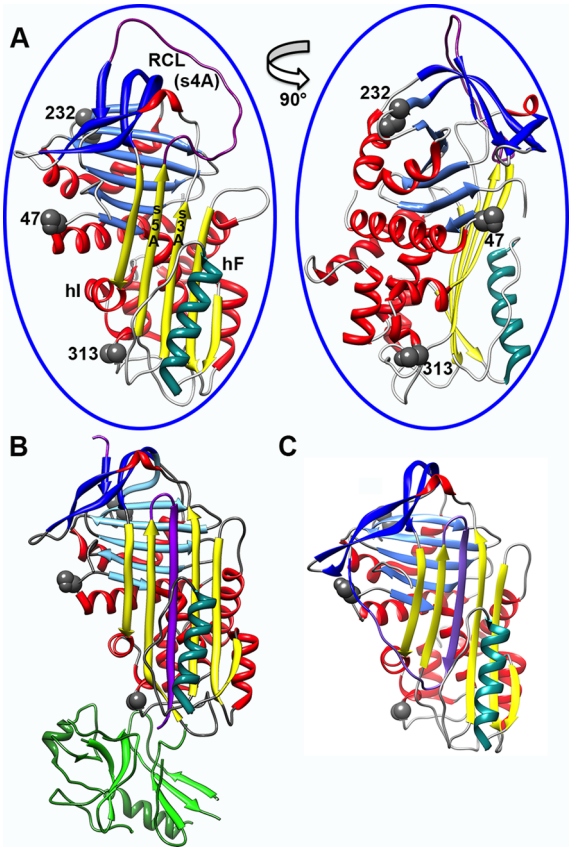

Figure 1. α_1AT anatomy and conformational gymnastics. (A) Two 90° views of the native α_1AT structure (PDB entry 1qlp[90]) showing β sheets A–C colored yellow, light blue, and blue, respectively, helix F colored turquoise, and the RCL colored magenta. The labeled residues are shown as van der Waals spheres. As shown by the blue ellipses, the separation of residues 232 and 313 approximately coincides with the long axis of α_1AT while the separation of residues 232 and 47 is close to one of the short axes. (B) Covalent complex between α_1AT and bovine trypsin (green) (PDB entry 1ezx[4]). (C) Inactive, latent serpin conformation of α_1AT (PDB entry 1iz2[10]). Protein images were generated using UCSF Chimera.[91]

insertion of the RCL and/or other β strands into an adjacent serpin.[12−16]

The watermelon shape or asphericity of crystallized serpin conformations may be quantified using the asphericity, Δ, and shape, *S*, measures developed by Dima and Thirumalai, where $S = \Delta = 0$ for spheres.[17] For active, metastable α_1AT, $\Delta = 0.19 \pm 0.01$, where a positive Δ indicates that the protein is not spherical, and $S = 0.16 \pm 0.01$, where a positive *S* indicates a prolate (watermelon) shape. A high value of Δ is also observed for other serpins, making most active serpins more aspherical than >70% of the monomeric proteins studied by Dima and Thirumalai. Interestingly, while functional insertion of the cleaved RCL does not alter the asphericity of α_1AT, the values of *S* and Δ are unchanged, the latent conformation with its intact RCL is significantly less aspherical [$\Delta = 0.15$, and $S = 0.11$ (Table S1 of the Supporting Information)]. Similar trends are observed for the inhibitory human serpin plasminogen activator inhibitor 1 where the latent form[18,19] is significantly less aspherical than the active[18,20,21] or cleaved[22] forms. Nor is this trend confined to human serpins; the latent state of the inhibitory bacterial serpin tengpin[23] is also significantly less aspherical than the active state (Table S1 of the Supporting Information). These shared structural characteristics suggest that decreased asphericity may be a hallmark of lower-energy, nonproductive serpin conformations.

While permanent alterations in serpin asphericity are associated with inactivation, transient expansion of the serpin structure is required for loop insertion[24] and has also been implicated in polymerization[15,25] and equilibrium unfolding.[25] How then do serpins fold to the aspherical final structure while avoiding more stable and more spherical structures such as the latent state? Serpins have been shown to fold using a mechanism with at least three states[7,26] via a molten globule intermediate[25−28] that is associated with aggregation.[27,29] Previous studies of serpin folding indicate that structures oriented along the long axis unfold first,[25,30−36] emphasizing the importance of this axis for folding, function, and dysfunction. However, to the best of our knowledge, there are no direct measurements of changes in the overall dimensions of a serpin during unfolding.

In more general terms, do aspherical proteins fold and/or unfold differently along different axes? Previous experiments aimed at addressing structural anisotropies used mechanical force and showed that the force required for protein unfolding can depend on the axis along which the force is applied.[37−40] However, these experiments were performed on relatively spherical proteins ($\Delta < 0.1$, and $S < 0.06$), and the energy landscapes for mechanical unfolding with its directional perturbation of protein folds can be quite different than those for chemical denaturation, which acts isotropically.[41−44]

We have used single-pair Förster resonance energy transfer (spFRET) to monitor the chemically induced equilibrium unfolding and refolding of active α_1AT. spFRET data for two different α_1AT variants, one labeled approximately along one of the short axes and the second labeled approximately along the long axis, suggest that chemically denatured α_1AT unfolds and refolds via at least two intermediates and that formation of the molten globule intermediates involves collapse of the long axis and an increase in the time-averaged sphericity. In addition, as observed in spFRET experiments with other proteins,[45−47] the unfolded state expands, along all axes, as the denaturant concentration increases. These results indicate the importance of the serpin long axis for both function and folding.

EXPERIMENTAL PROCEDURES

Asphericity (Δ) and Shape (*S*) Parameters. Δ and *S* were calculated as described by Dima and Thirumalai[17] using Mathematica (Wolfram Research). The Mathematica scripts for reading the PDB file and performing the calculations were extensively modified versions of the Mathematica notebook Inertiatensor.[48] All of the calculated values are listed in Table S1 of the Supporting Information.

α_1AT Preparation and Labeling. Wild-type α_1AT contains a single Cys at position 232. To create double-Cys variants for spFRET experiments, a second Cys was introduced into the wild-type background, Ser47Cys (2Cys47) or Ser313Cys (2Cys313), in plasmid pEAT8-137[49,50] using the Quikchange XL (Agilent) site-directed mutagenesis protocol. Control fluorescence experiments required single-Cys variants: wild-type (containing Cys232), Ser47Cys/Cys232Ser (S47C), and Ser313Cys/Cys232Ser (S313C). The previously characterized single-Cys variants, S47C and S313C, do not alter α_1AT stability or activity.[31,51] All double- and single-Cys α_1AT variants were expressed as inclusion bodies in *Escherichia coli* BL21(DE3) cells, refolded, and purified as previously

dx.doi.org/10.1021/bi401622n | *Biochemistry* 2014, 53, 2903−2914

described.[51] For all α_1AT variants, this procedure yielded protein that was >98% pure as judged by sodium dodecyl sulfate−polyacrylamide gel electrophoresis and gel densitometry.

Single-Cys variants were labeled with the donor Alexa Fluor 488 maleimide (AF488) (Invitrogen) or the acceptor Texas Red maleimide (TR) (Invitrogen) according to the manufacturer's instructions. Double-Cys variants were first labeled with AF488, using a 1:1 dye:protein ratio. For spFRET measurements, a MonoQ anion exchange column (GE Healthcare) was used to separate singly labeled protein from unlabeled and doubly labeled species. The resulting singly labeled protein was further labeled with TR according to the manufacturer's instructions. Labeling efficiencies for both fluorophores were measured by absorption according to the manufacturer's instructions. For the doubly labeled variants, the shorter labeling time used for AF488 (donor), to avoid double labeling, resulted in 80−100% labeling, while longer labeling times used for TR (acceptor) labeling resulted in approximately 100% labeling. Single-Cys variants S47C and S313C were >70% labeled by both AF488 and TR. In contrast, the wild-type, with a single Cys at position 232, was >70% labeled by TR, but only ∼10% labeled using AF488. These results indicate that most of the doubly labeled α_1AT variants have the acceptor, TR, attached to Cys232 and the donor, AF488, attached to either residue 47 or 313.

The stoichiometry of inhibition (SI), the number of moles of α_1AT needed to inhibit bovine trypsin (Sigma-Aldrich), was determined as previously described.[51] Wild-type α_1AT has an SI of 1.0, while the SI is 1.1 for unlabeled and labeled single- and double-Cys variants.

Far-UV Circular Dichroism (CD). Room-temperature far-UV CD spectra from 200 to 250 nm were recorded on a Jasco J-810 spectropolarimeter using a 0.1 cm path length at room temperature. Samples containing 1.8 μM α_1AT variants in 10 mM sodium phosphate (pH 7.4) and 50 mM NaCl with 0−6 M guanidinium chloride (GdmCl) were equilibrated for 2 h. GdmCl concentrations were determined from the index of refraction.[52] In 0 M GdmCl, the spectra of folded, doubly labeled Cys variants are essentially identical to that of wild-type α_1AT, indicating that the mutations do not significantly alter the α_1AT structure (Figure 2). The apparent fraction of unfolded protein, f_{app}, was determined from the far-UV CD unfolding data:

$$f_{app} = \frac{\theta_{222} - \theta_{222,N}}{\theta_{222,U} - \theta_{222,N}} \quad (1)$$

where θ_{222} is the measured ellipticity at 222 nm, N is the native, fully folded protein in 0 M GdmCl, and U is the unfolded protein in 6 M GdmCl. f_{app} was fit to a three-state model for unfolding[53] (Supporting Information and Table S2).

Steady State Fluorescence Spectra and Anisotropies. Increasing concentrations of GdmCl and/or protein unfolding can alter the absorption and emission spectra as well as the quantum yields of the fluorophores, potentially changing R_o, the Förster distance at which there is 50% energy transfer. To account for these effects, the steady state absorption spectra (data not shown), fluorescence emission spectra (data not shown), and steady state fluorescence anisotropies (Figure S1 of the Supporting Information) were measured for all three single-Cys variants labeled with AF488 or TR. Absorption spectra were collected using a UV−vis spectrometer

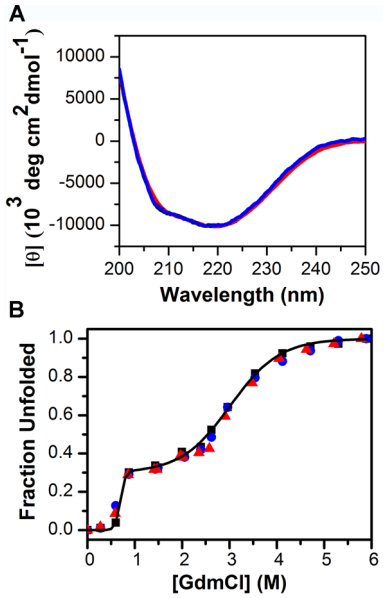

Figure 2. α_1AT structure and stability not significantly affected by Cys mutations and fluorescent labeling. (A) Far-UV CD spectra of the native state of wild-type (black), doubly labeled 2Cys47 (blue), and doubly labeled 2Cys313 (red) α_1AT in 10 mM sodium phosphate (pH 7.4) and 50 mM NaCl. (B) GdmCl-induced unfolding of α_1AT monitored by far-UV CD for the wild-type (black squares), doubly labeled 2Cys47 (blue circles), and doubly labeled 2Cys313 (red triangles). The line is a three-state fit to the wild-type data (Supporting Information and Table S2).

(PerkinElmer), while fluorescence spectra and steady state anisotropy data were collected using a Fluorolog fluorometer (ISA) as previously described.[51] Singly labeled α_1AT variants were incubated in 50 mM HEPES (pH 7.4), 50 mM NaCl, 0.01% Tween 20 buffer containing 0−6 M GdmCl for 2 h at room temperature to reach equilibrium.[31] Surprisingly, both the AF488 emission spectra and the TR absorption spectra red shift with an increasing GdmCl concentration, resulting in a very slight dependence of R_o on the GdmCl concentration (Figure S2 of the Supporting Information).

The effective value of R_o in the spFRET experiments, $R_{o,eff}$, is influenced by differences in quantum yield and detection efficiency between the donor (AF488) and acceptor (TR) as[54]

$$R_{o,eff} = \gamma^{1/6} R_o \quad (2)$$

For singly labeled samples with identical optical densities at the donor excitation wavelength, 488 nm, γ is the ratio of the fluorescence intensity of the acceptor-only samples to that of donor-only samples measured on the single-molecule setup[46] and γ was measured as a function of GdmCl concentration (Figure S2 of the Supporting Information). Analytically, $\gamma = (\phi_A \eta_A)/(\phi_D \eta_D)$, where A and D refer to the donor and acceptor, respectively, ϕ is the quantum yield, and η is the detection efficiency.[55] The resulting $R_{o,eff}$ is 51 Å for all GdmCl concentrations (Figure S2 of the Supporting Information).

spFRET Data Collection and Analysis. Doubly labeled α_1AT variants were incubated in 50 mM HEPES (pH 7.4), 50 mM NaCl, 0.01% Tween 20 buffer containing 0−6 M GdmCl for 2 h at room temperature to reach equilibrium.[31] After 2 h, the micromolar samples were diluted to <50 pM for spFRET experiments. For refolding experiments, α_1AT variants were

dx.doi.org/10.1021/bi401622n | Biochemistry 2014, 53, 2903−2914

first unfolded in buffer containing 8 M GdmCl for 2 h and then allowed to refold in 0−6 M GdmCl for 2 h.

spFRET data were collected on a home-built confocal microscope based on an IX-70 inverted microscope (Olympus) that has been previously described[51,55] (and Supporting Information). Data from the donor and acceptor channels were binned at 1 kHz, and a threshold of 30 total (acceptor plus donor) photon counts was used to identify photon bursts arising from α_1AT diffusing through the focal volume. The apparent spFRET efficiency, E_{app}, for these bursts was calculated using[55,56]

$$E_{app} = \frac{I_A}{I_A + I_D} \tag{3}$$

where I_A is the photon count for the acceptor corrected for background and leakage of donor photons into the acceptor channel (crosstalk) and I_D is the photon count for the donor corrected for background. The apparent mean spFRET efficiency, $\langle E_m \rangle$, and the peak half-width, σ_m, were determined from Gaussian fits to the data. The upper bound for peak half-widths, σ_{sn}, due to shot noise were calculated using[56,57]

$$\sigma_{sn} \leq \sqrt{[\langle E_m \rangle (1 - \langle E_m \rangle)]/P_t} \tag{4}$$

where P_t = 30 photon counts (donor + acceptor) is the threshold used to identify photon bursts arising from single α_1AT molecules traversing the observation volume.

Radius of Gyration of the Denatured State Ensemble (DSE). Assuming that unfolded α_1AT behaves as a Gaussian chain, the average radius of gyration of the DSE, R_g, can be calculated from the mean square distance between the dyes, $\langle r^2 \rangle$:[58]

$$R_g = \sqrt{\frac{N_t}{N_{dyes}} \frac{\langle r^2 \rangle}{6}} \tag{5}$$

where N_t is the total number of peptide bonds in the protein (393 for α_1AT) and N_{dyes} is the number of peptide bonds between the donor and acceptor fluorophores. AF488 has a five-carbon linker, while TR maleimide has a two-carbon linker adding the equivalent of three peptide bonds between the donor and acceptor. The mean square distance between the dyes, $\langle r^2 \rangle$, can be determined from $\langle E_{m,\gamma} \rangle$ for the DSE according to[47,59]

$$\langle E_{m,\gamma} \rangle = \int_c^{l_c} E(r) P(r)\, dr \tag{6}$$

$$E(r) = \left[1 + \left(\frac{r}{R_{o,eff}}\right)^6\right]^{-1} \tag{7}$$

$$P(r) = 4\pi r^2 \left(\frac{3}{2\pi \langle r^2 \rangle}\right)^{3/2} e^{-3r^2/2\langle r^2 \rangle} \tag{8}$$

where c is the distance of closest approach, l_c is the contour length between the fluorophores, assuming 0.38 nm per peptide bond,[60] r is the distance between the fluorophores, $E(r)$ is the energy transfer efficiency at distance r, and $P(r)$ is the probability of observing a particular distance assuming that the unfolded protein behaves as a Gaussian chain. The Gaussian chain approximation assumes that the DSE behaves as an ideal freely jointed polymer with negligible interactions between amino acids. This model allows us to calculate the approximate radius of gyration but neglects confounding factors such as residual structure in the DSE. Note that to obtain distances from the FRET efficiencies, it is necessary to correct for differences in quantum yield and detection efficiency between the donor (AF488) and the acceptor (TR) given by γ, and $\langle E_{m,\gamma} \rangle$ is the γ-corrected apparent mean FRET efficiency, $\langle E_{m,\gamma} \rangle = \langle E_m \rangle / [\langle E_m \rangle + \gamma(1 - \langle E_m \rangle)]$. (The FRET efficiency histograms were not γ-corrected because the relationship between the γ-corrected efficiencies and the counts in a histogram bin is not straightforward.[56]) For these experiments, γ varied from 0.85 in 0 M GdmCl to 0.95 in 6 M GdmCl (Figure S2 of the Supporting Information). To determine the value of $\langle r^2 \rangle$ associated with $\langle E_{m,\gamma} \rangle$ for each concentration of GdmCl, eq 6 was numerically integrated using Mathematica for various values of $\langle r^2 \rangle$. For each denaturant concentration, the R_g of the DSE was calculated using the value of $\langle r^2 \rangle$ for which the numerical integral matched the experimentally observed values of $\langle E_{m,\gamma} \rangle$.

Fluorescence Correlation Spectroscopy (FCS). FCS was used to monitor α_1AT translational diffusion and to look for conformational changes on time scales faster than that of diffusion through the observation volume. The correlations, $G_{jk}(\tau)$, were calculated by the ISS Vista program according to[61,62]

$$G_{jk}(\tau) = \frac{\langle \delta I_j(t) \delta I_k(t + \tau) \rangle}{\langle I_j(t) \rangle \langle I_k(t) \rangle} \tag{9}$$

where the broken brackets denote the time average, $I_j(t)$ is the photon count for channel j, and $\delta I_j(t) = \langle I_j(t) \rangle - I_j(t)$. $j = k$ for the autocorrelation, while $j \neq k$ for the crosscorrelation.

The correlations were calculated using the photon counts from the spFRET experiments, collected with a 100 μm confocal pinhole. Additional FCS experiments were performed as previously described[63] using a 30 or 100 μm confocal pinhole and α_1AT variants labeled only with the donor or with the donor and acceptor fluorophores. The ratio of the donor autocorrelation to the donor−acceptor crosscorrelation, $G_{DD}(\tau)/G_{DA}(\tau)$, for spFRET−FCS experiments and the ratio of the fluorescence autocorrelation of the donor, $G_{DD}(\tau)$, in the presence and absence of acceptor fluorophore for FCS-only experiments were calculated using Origin (OriginLab).

To determine diffusion times, τ_D, correlation curves for α_1AT variants labeled only with the donor fluorophore, AF488, were fit to[62]

$$G(\tau) = \frac{1}{\langle N \rangle}\left[1 + \frac{F}{1 - F}\exp\left(-\frac{\tau}{\tau_{dark}}\right)\right] \left[\left(1 + \frac{\tau}{\tau_D}\right)^{-1}\left(1 + \frac{\tau}{S^2 \tau_D}\right)^{-1/2}\right] \tag{10}$$

where $\langle N \rangle$ is the effective number of molecules in the observation volume and the exponential expression accounts for AF488 fluorophores that are nonfluorescent due to quenching interactions. F is the fraction of molecules residing in the dark state at any time, and τ_{dark} is the lifetime of the dark state. The last term accounts for fluorescence fluctuations due to translational diffusion with $\tau_D = \omega_o^2/D$ where ω_o is the radius of the three-dimensional Gaussian observation volume and $S = z_o/\omega_o$ is the ratio of the axial to the radial extent. S and

dx.doi.org/10.1021/bi401622n | Biochemistry 2014, 53, 2903−2914

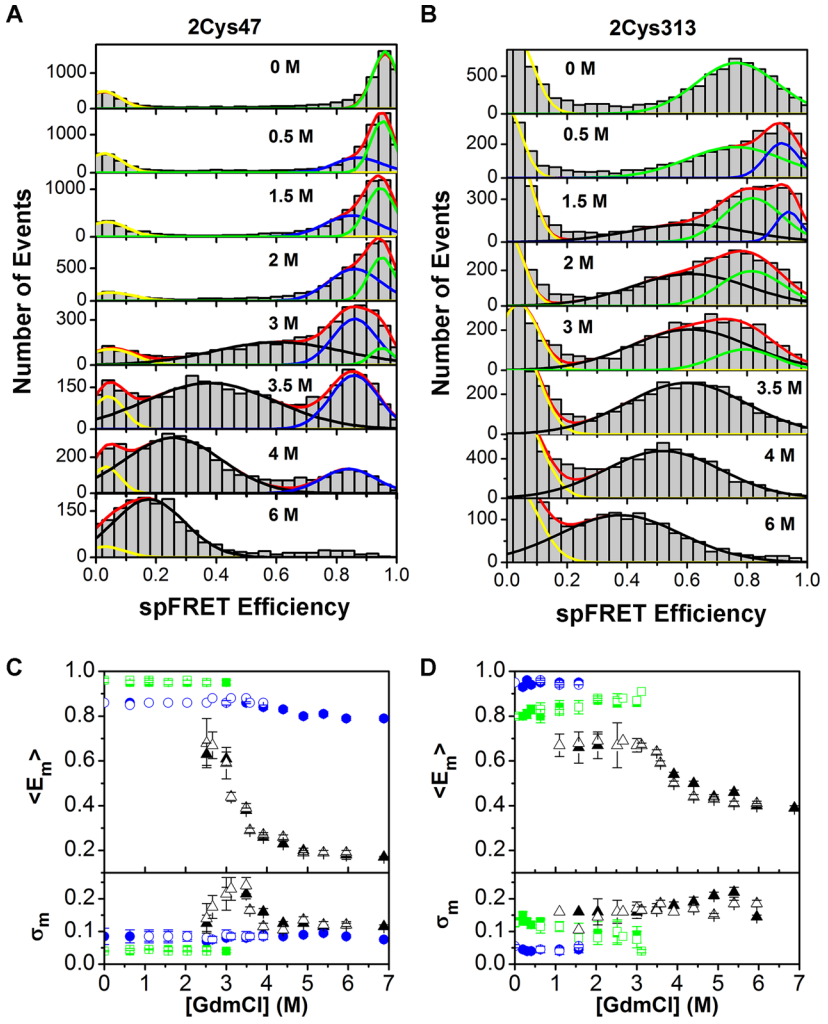

Figure 3. α_1AT unfolding is different along the short and long axes. spFRET histograms for the unfolding of 2Cys47 (A) and 2Cys313 (B) in increasing concentrations of GdmCl as indicated on the plots. The total Gaussian fits to the histograms are indicated by red lines, and the resulting single Gaussians for the native, intermediate, unfolded, and zero peaks are indicated by green, blue, black, and yellow lines, respectively. The distance between residues 232 and 47 (2Cys47) increases as α_1AT unfolds, while the distance between residues 232 and 313 (2Cys313) first decreases and then increases. (C and D) Centers, $\langle E_m \rangle$, and half-widths, σ_m, of the spFRET peaks, determined from the Gaussian fits, as a function of GdmCl concentration for 2Cys47 (C) and 2Cys313 (D). Data for the native, intermediate, and unfolded species are colored green, blue, and black, respectively. Filled symbols were determined from unfolding experiments, while empty symbols were determined from refolding experiments.

ω_o were determined from FCS experiments using Alexa Fluor 488 hydrazide as a diffusion standard.

The correlation curves also allowed us to easily check for α_1AT aggregation because such aggregates will diffuse slowly and have large values of τ_D. Increases in τ_D were observed as α_1AT expanded due to unfolding, but these increases were within the range expected for increased viscosity at higher GdmCl concentrations and chain expansion. Large deviations and bumps, the hallmarks of significant aggregation, were not observed (data not shown). Using the 100 μm pinhole, the diffusion time of native α_1AT in the absence of GdmCl was 240 ± 20 μs and τ_D increased to 550 ± 50 μs in 5 M GdmCl, reflecting both a 1.3-fold increase in viscosity and α_1AT unfolding.

RESULTS

To monitor changes in the shape of α_1AT during equilibrium unfolding, the donor (AF488) and acceptor (TR) fluorophores for spFRET were placed approximately along either a short axis or the long axis (Figure 1). α_1AT has a single native Cys, residue 232, located at the C-terminal end of β sheet B strand 1 (s1B), and this Cys was labeled in all of the variants. For the short axis variant, 2Cys47, the second Cys, located in a short loop between helix A and s6B, was introduced by mutating Ser47 to Cys, resulting in a donor−acceptor separation of ∼27 Å in the native state. For the long axis variant, 2CyS313, Ser313, located in a flexible region[64] near β sheet A, was mutated to Cys, resulting in a donor−acceptor separation of ∼43 Å in the native state. All of the labeled variants were active, inhibiting bovine trypsin with an SI of 1.1 similar to that of the wild-type.

Stability of the Labeled α_1AT Variants. The stability of wild-type α_1AT and its labeled variants was monitored using far-UV CD. As expected, on the basis of previous ensemble studies of α_1AT unfolding,[7,26,31,65] α_1AT unfolding is biphasic as indicated by the plateau around 1 M GdmCl (Figure 2). The Cys mutations and double labeling do not significantly alter the α_1AT stability, and fits to the far-UV CD unfolding curves are similar for the wild-type and doubly labeled variants (Figure 2 and Table S2 of the Supporting Information).

dx.doi.org/10.1021/bi401622n | Biochemistry 2014, 53, 2903−2914

Table 1. Changes in the Peak Centers and Widths for the α_1AT DSE[a]

[GdmCl] (M)	2Cys47 $\langle E_m \rangle$[b]	2Cys47 σ_m[b]	2Cys47 σ_{sn}	2Cys313 $\langle E_m \rangle$[b]	2Cys313 σ_m[b]	2Cys313 σ_{sn}
1.5	NA[c]	NA[c]	NA[c]	0.61 (0.02)	0.16 (0.01)	0.09
2	NA[c]	NA[c]	NA[c]	0.61 (0.02)	0.16 (0.01)	0.09
2.5	0.63 (0.02)	0.13 (0.01)	0.09	0.62 (0.02)	0.17 (0.01)	0.09
3	0.61 (0.01)	0.22 (0.01)	0.09	0.62 (0.01)	0.16 (0.01)	0.09
3.5	0.38 (0.01)	0.22 (0.01)	0.09	0.61 (0.01)	0.18 (0.01)	0.09
4	0.26 (0.01)	0.16 (0.01)	0.08	0.52 (0.01)	0.18 (0.01)	0.09
5	0.20 (0.01)	0.13 (0.01)	0.07	0.40 (0.01)	0.18 (0.01)	0.09
6	0.18 (0.01)	0.12 (0.01)	0.07	0.38 (0.01)	0.19 (0.01)	0.09

[a]Peak centers, $\langle E_m \rangle$, and half-widths, σ_m, were determined from Gaussian fits to the unfolded peaks in the spFRET histograms. The predicted half-widths from shot noise, σ_{sn}, were calculated according to eq 4.[56,57] [b]The number in parentheses is the standard deviation from fits to histograms from at least two independent spFRET experiments. [c]Not Applicable. For 2Cys47, the DSE is not observed at moderate GdmCl concentrations.

Unfolding along the Short Axis. In 0 M GdmCl, spFRET histograms for doubly labeled 2Cys47 show two peaks, a small, "zero" peak arising from proteins containing only AF488 (donor) and proteins in which TR (acceptor) has photobleached as well as a much larger peak with an apparent mean efficiency, $\langle E_m \rangle$, of 0.95 (0.96 when corrected for γ) (Figure 3A). The short distance, ~27 Å, between residue 47 and Cys232 in the native structure would yield a native state spFRET signal centered at 0.97. However, the five-carbon (AF488) or two-carbon (TR) flexible chains linking the fluorophores to the Cys residues can increase this distance, and the peak centered at 0.95 efficiency with a half-width of 0.04 can easily be assigned to the α_1AT native state (Figure 3A).

As expected from the ensemble experiments, as the concentration of GdmCl increases to 0.5 M, a third peak appears in the spFRET histogram centered at 0.85. Because of its appearance at low GdmCl concentrations, and the subsequent appearance of a fourth lower-efficiency peak at even higher concentrations of denaturant, this $\langle E_m \rangle = 0.85$ peak must arise from equilibrium unfolding intermediates. The flexibility of the region around the fluorophores can increase the range of interfluorophore distances that can be sampled, thus increasing the width of the spFRET peaks. The spFRET peaks centered at 0.85 have half-widths of 0.08, only slightly higher than the half-width of 0.07 predicted from shot noise.[56,57] The α_1AT equilibrium folding intermediate, which has been characterized as a molten globule,[25−28] should be able to access multiple conformations leading to a spFRET peak wider than what would be predicted simply from shot noise. However, the observed difference between the predicted half-width and the measured half-width is quite small and likely arises from experimental noise. The lack of resolvable heterogeneity for the separation between fluorophores at residues 232 and 47 illustrates the limits of the spFRET measurements. Because FRET has an r^{-6} distance dependence, FRET measurements are most sensitive between efficiencies of 0.8 and 0.2 (40.5 to 64.3 Å for an R_o of 51 Å), and much less sensitive at the extremes. Thus, conformational heterogeneity of the intermediate state(s) that changes the separation between residues 232 and 47 by ~3.5 Å or less will be masked by noise for an spFRET efficiency peak centered at 0.85.

Around 2.5 M GdmCl, a fourth peak appears centered at 0.65. However, unlike the native and intermediate states, for which the peak centers are independent of denaturant concentration, the center of this peak, arising from the DSE, shifts to lower efficiencies as the GdmCl concentration increases (Figure 3A,B and Table 1). These DSE peaks are considerably wider than what would be predicted from shot noise. Using an $R_{o,eff}$ of 51 Å to convert the spFRET efficiency peak half-widths to approximate distance changes between the fluorophores reveals that these large half-widths change the fluorophore separation by more than 5 Å. Thus, while experimental noise makes a small contribution to these half-widths, the widths of the spFRET peaks for the DSE likely reflect conformational heterogeneity (Table 1). Such heterogeneity could arise from metastable states separated by low-energy barriers,[66,67] i.e., states with lifetimes longer than the time it takes to diffuse through the observation volume, ~1 ms.

The decrease in the apparent efficiency as the denatured states expand in increasing concentrations of GdmCl is commonly observed in spFRET unfolding experiments[45−47,54,68,69] and is expected due to solvation of the polypeptide chain.[47,69] At low GdmCl concentrations, more compact configurations are favored because of interactions between amino acids, but at higher denaturant concentrations, solvent−amino acid interactions dominate and the unfolded states are, on average, more extended.[45,47,69] The unfolding of 2Cys47 is reversible, and the locations of the spFRET peaks for the native, intermediate, and unfolded ensembles are the same for equilibrium unfolding and refolding (Figure S3 of the Supporting Information). Thus, spFRET measurements approximately along one of the short axes show the expected three-state unfolding and reveal that the intermediate and unfolded ensembles are distinct conformational ensembles separated by an energy barrier.

Unfolding along the Long Axis. In 0 M GdmCl, the spFRET histogram for doubly labeled 2Cys313 displays two peaks, the zero peak and a peak centered at an apparent efficiency of 0.80 (0.82 when corrected for γ) corresponding to the native state (Figure 3B). The half-width of the native state peak is 0.14, considerably wider than the half-width of 0.07 that would be predicted from shot noise. This large half-width indicates significant flexibility around and/or between residues 232 and 313. Cys232 is at the end of s1B, and the region from residue 232 to 313 contains four β strands and three α helices (s2B−s3B−αG−αH−s2C−s6A−αI). Data from mass spectrometry experiments including hydrogen−deuterium exchange mass spectrometry (HDXMS) and oxidative labeling[25,33,64] as well as PEGylation of single introduced buried Cys residues as a function of GdmCl concentration[32] suggest that β sheet B is quite stable and that the region from residue 275 to 313 (end of αH to 313) is more labile with large fluctuations likely in the loopy hI−s5A region (residues 299−331).

The effects of loop motions on the spFRET peak shape, location, and width depend on the time scale of the motion

dx.doi.org/10.1021/bi401622n | Biochemistry 2014, 53, 2903−2914

relative to the time it takes α_1AT to diffuse through the observation volume (~475 μs) and the bin time used for the histogram (1 ms).[56] On the basis of these time scales, loop conformational changes that are ~200 μs or longer would likely increase the peak width. Modeling long-time scale protein fluctuations using coarse graining combined with Monte Carlo methods as implemented by the CABS-flex Web server[70,71] suggests that the hI−s5A loop may occasionally fold back on itself, allowing it to populate both less flexible and more flexible metastable states perhaps accounting for the large width of the 2Cys313 native spFRET peak (data not shown).

Surprisingly, as the GdmCl concentration is increased, a third peak appears to be centered at a higher spFRET efficiency of 0.95, corresponding to a decrease in the distance between the two fluorophores. This contraction is not due to fluorescence artifacts, because the absorption and emission characteristics of AF488 and TR do not significantly change from 0 to 3 M GdmCl (Figures S1 and S2 of the Supporting Information). This signal must, therefore, arise from intermediates in equilibrium folding for which the long axis has contracted relative to the native, folded structure. Note that the relative insensitivity of FRET to distance changes at such high efficiencies results in very narrow peak widths despite the conformational heterogeneity observed for the 2Cys313 native state and expected for the intermediate ensemble.

For the 2Cys47 α_1AT variant, the location of the native state peak is independent of denaturant concentration (Figure 3). However, when the 2Cys313 α_1AT variant was incubated in higher concentrations of GdmCl, expansion of the intermediate ensemble made it difficult to distinguish between spFRET signals arising from intermediate conformations and those arising from the native state with its intact long axis. At 0.85 M GdmCl, the center of the 2Cys313 peak center assigned to the native state shifts from an apparent efficiency of 0.80 to 0.86. The location of this peak, between the intermediate peak at 0.95 and the original native peak at 0.80, suggests that two intermediate ensembles may be populated.

Unlike 2Cys47, in which an unfolded state peak does not appear until ~2 M GdmCl, for 2Cys313 an unfolded peak appears at 1.5 M GdmCl, revealing that the region between residues 232 and 313 likely unfolds at denaturant concentrations lower than those for the region between residues 232 and 47. As observed for the 2Cys47 unfolded peak, the apparent spFRET peak efficiency for the 2Cys313 unfolded peak decreases with increasing GdmCl concentrations, and the half-widths are wider than those predicted from shot noise (Figure 3D and Table 1). These results are consistent with previous ensemble fluorescence experiments indicating that the region around residue 313 unfolds in low GdmCl concentrations,[31] and that the region near Trp238 in strand 2B, within 10 Å of Cys232, unfolds only at high GdmCl concentrations.[34] In addition, equilibrium unfolding studies of α_1AT variants in which buried residues were mutated to Cys and the exposure of buried residues was probed by reactivity with high-molecular weight poly(ethylene glycol)-maleimide (PEG-Mal) revealed that residue 302 in helix I (15 Å from residue 313) and residue 332 in strand 5A (13 Å from residue 313) are fully accessible to PEG-Mal at GdmCl concentrations of <1 M while residue 237 in strand 2B (6 Å from residue 232) is fully accessible only at GdmCl concentrations of >2.5 M.[32] Thus, multiple probes of folding show that the helix I to strand 5A region containing residue 313 is quite labile while β sheet B containing residue 232 is much more stable.

The unfolding of 2Cys313 is reversible, and peak centers and half-widths similar to those observed upon unfolding are observed upon refolding (Figure S3 of the Supporting Information). The 2Cys47 and 2Cys313 results suggest that the α_1AT long axis and short axes behave differently during equilibrium unfolding and refolding. The monitored short axis shows the expected expansion as the protein unfolds via the intermediate; in contrast, the long axis contracts in the initial folding intermediates and then expands upon further unfolding.

Characterizing the DSE. Fully denatured proteins can be modeled as unstructured, random polymer chains with mean square end-to-end distances that follow a Gaussian distribution.[45,47,59,72−74] In this model, a Gaussian distribution also describes the root-mean-square distance between donor and acceptor fluorophores separated by ≥80 amino acids. The Gaussian chain model and eqs 5−8 can then be used to determine the radius of gyration, R_g, which should be the same for both the short and long axis spFRET variants if the denatured states are truly unstructured polymers. Above 3.5 M GdmCl, the radii of gyration determined from the γ-corrected centers of the unfolded peaks are similar for both 2Cys47 and 2Cys313, confirming that the time-averaged α_1AT conformation is no longer asymmetric (Figure 4). As observed for other

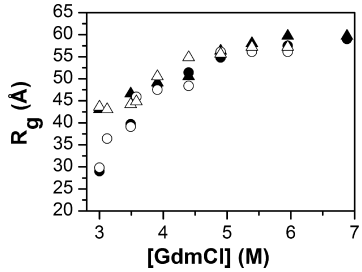

Figure 4. Radius of gyration (R_g) tracks α_1AT expansion with increasing GdmCl concentrations. R_g calculated from 2Cys47 spFRET histograms (circles) and 2Cys313 spFRET histograms (triangles). The filled symbols were calculated from unfolding experiments, and the empty symbols were calculated from refolding experiments.

proteins, the R_g of the DSE increases with increasing concentrations of GdmCl.[75,76] In 6 M GdmCl, the R_g is 58 ± 2 Å, a 145% increase relative to the R_g of 23.7 Å measured by small angle neutron scattering for the native state.[77]

Limits on the Kinetics of Interconversion between States. While the equilibrium spFRET data provide information about conformational distributions, the time scales of fluorescence fluctuations due to translational diffusion and fast structural fluctuations may be determined using FCS.[61,62,78,79] At low protein concentrations, diffusion of fluorescent proteins in and out of the observation volume leads to fluorescence fluctuations on the time scale of diffusion (hundreds of microseconds) that are reflected in the decay of the correlation function (Figure S4A of the Supporting Information).[61,62] Fluorescence fluctuations on time scales faster than that of diffusion, arising, for example, from significant structural fluctuations that alter the donor to acceptor distance, will lead to exponential decays of the correlation with time constants of microseconds or longer in addition to the contributions from diffusion and fluorophore photochemistry (eq 10).[62,78,80−82] In the absence of dynamic changes in distance between the donor and acceptor, the fluorescence correlation can be expressed as $G_1(\tau) = G_{pc}(\tau)$

$G_{diff}(\tau)$, which has contributions from diffusion, $G_{diff}(\tau)$, and photochemistry such as excursions into the triplet states and quenching by Trp residues, $G_{pc}(\tau)$ (see eq 10). In the presence of structural dynamics that alter the distance between the donor and acceptor fluorophores, an additional term, $G_{dynamics}(\tau)$, contributes to the fluorescence fluctuations and the correlation function can be expressed as $G_2(\tau) = G_{dynamics}(\tau)G_{pc}(\tau)G_{diff}(\tau)$. The ratio between these functions will reveal the time scale(s) of the structural fluctuations:[78,80−82]

$$\frac{G_2(\tau)}{G_1(\tau)} = \frac{G_{dynamics}(\tau)G_{pc}(\tau)G_{diff}(\tau)}{G_{pc}(\tau)G_{diff}(\tau)} = G_{dynamics}(\tau) \quad (11)$$

This ratio may be calculated in two ways: (i) the donor autocorrelation for protein labeled with both the donor and acceptor may be divided by the crosscorrelation between the donor and acceptor channels,[82] or (ii) the donor autocorrelation for protein labeled with both the donor and acceptor may be divided by the donor autocorrelation for protein labeled only with the donor. In both of these cases, the diffusion and photochemistry contributions should cancel out and the contribution of fluorescence fluctuations due to conformational changes should be obvious.[80,82]

To put limits on how fast α_1AT can interconvert between states, we performed FCS experiments on α_1AT labeled only with the donor, AF488, and on α_1AT labeled with both the donor, AF488, and the acceptor, TR, for both 2Cys47 and 2Cys313 and calculated both types of ratios. The resulting ratios are essentially flat and similar for all concentrations of GdmCl, including 0 M GdmCl (Figure S4 of the Supporting Information). These results indicate that the average interconversion between states occurs more slowly than diffusion through the observation volume. This puts a lower limit of ∼250 μs for interconversion between the folded and intermediate ensembles and of ∼500 μs for interconversion between the intermediate ensemble and the DSE. (The approximate doubling of the diffusion time arises from both the increase in viscosity at higher GdmCl concentrations and expansion associated with unfolding.)

DISCUSSION

Native α_1AT is a watermelon-shaped ellipsoid. In 2Cys47, the two fluorophores are located approximately along one of the short axes of the ellipsoid, while in 2Cys313, the two fluorophores are close to the long axis (Figure 1). By combining these labeling schemes with spFRET, we tracked the overall symmetry of α_1AT during equilibrium unfolding and refolding. The spFRET histograms were calculated for data binned at 1 kHz, and the shape of α_1AT is therefore averaged over the time (hundreds of microseconds) it takes for the molecules to traverse the observation volume. This is particularly important for the DSE at high GdmCl concentrations where the instantaneous conformation of unfolded α_1AT can be quite extended and aspherical, but the lack of preferred conformations leads to a relatively spherical time-averaged conformation. Our time-averaged results indicate that the first events in equilibrium unfolding involve contraction of the long axis and expansion of the short axes, resulting in a more spherical overall conformation, followed by overall expansion of α_1AT as shown in Scheme 1, in which the dots indicate the approximate locations of the fluorophores; N, I_1, I_2, and U indicate the native, intermediate, and denatured state ensembles, respectively; and the braces denote the heterogeneity of the intermediate ensembles and the DSE.

Scheme 1. α_1AT Equilibrium Folding Showing the Initial Compaction of the Long Axis and Expansion of the Short Axes

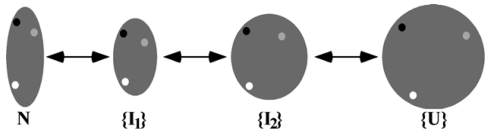

A number of α_1AT equilibrium unfolding studies suggest that the unfolding intermediates are classic molten globules[25,27,28] with a compact conformation, and significant, but fluctuating, secondary structure.[83] For α_1AT, GdmCl-induced equilibrium intermediates show significant secondary structure as determined by far-UV CD[7,28,31] (Figure 2), and the backbone amide hydrogens throughout the protein show no significant protection from hydrogen exchange [with the exception of a peptide in sheet B (residues 241−251) that shows some protection up to 4 M GdmCl], indicating that the structure fluctuates, and no significant heat capacity peak is observed for the transition between the intermediates and the unfolded states in differential scanning calorimetry (DSC) experiments.[25] Collapse of some structural constraints is also supported by the accessibility of buried Cys residues in helix I, s5A, and helix F regions to PEGylation even at low GdmCl concentrations.[32] Residue 313 is in the helix I−turn−s5A region, and the 2Cys313 spFRET results, which report on the lability of the long axis in this region, clearly agree with the HDXMS[25] and PEGylation[32] results at low GdmCl concentrations (<1 M) as well as the significant stabilization afforded by mutating Lys335 in s5A to small residues (Ala, Gly, and Val).[8,84,85] Overall, the decrease in asphericity observed for the intermediates is entirely consistent with the intermediates' molten globule character because relaxation of the anisotropic constraints imposed by the tertiary structure will increase the overall, time-averaged symmetry during serpin unfolding.

Compared to the region around residue 313, the helix A−strand 6B region containing residue 47 is more stable. It is accessible to PEGylation only above 1 M GdmCl[32] and gains 40−60% protection from hydrogen−deuterium exchange[35] and oxidative labeling[33] after refolding for ∼10 min. The 2Cys47 spFRET histogram even shows a small native state peak for 2Cys47 at 3 M GdmCl (Figure 3A), suggesting that some regions of α_1AT retain small but significant amounts of native state character even in the presence of moderate to high denaturant concentrations. This retention of local tertiary constraints is supported by HDXMS data for the peptide containing residues 241−251 that is not fully exchanged even at 4 M GdmCl, indicating the presence of some hydrogen bonding in β sheet B[25] and the lack of complete PEGylation at 3 M GdmCl for the Cys residues introduced at positions 55 and 65, near Ser47, and at position 237, near Cys232.[32] In addition, fluorescence from Trp238, near Cys232, shows only one transition with unfolding midpoints at 5.3 M for urea denaturation and 1.8 M for guanidinium sulfate denaturation, again indicating the retention of local native state character in β sheet B even at high denaturant concentrations. The higher local stability reported by 2Cys47 is also evident in the intermediate ensemble(s); the 2Cys47 intermediate ensemble shows significant population even at 4 M GdmCl where the 2Cys313 histogram shows only the DSE (Figure 3).

These differences in the spFRET histograms are consistent with the greater stability of the short axis monitored in the 2Cys47 experiments relative to the long axis monitored in the 2Cys313 experiments. Differences in stability between the 2Cys313 and 2Cys47 intermediate ensembles suggest that the s1B−s2B region probed by Cys232 in both constructs is quite stable. As discussed above, the stability of this region is further supported by fluorescence data from the Trp residue in s2B (Trp238),[34] PEGylation data,[32] and the early acquisition of structure in this region during kinetic experiments.[33,35] Thus, the B/C barrel region is the most stable part of α_1AT. All of these data, along with fragment complementation studies that lead to stable, folded serpins for both α_1AT[86] and ovalbumin,[87] support a model of α_1AT equilibrium folding in which secondary structure formation at moderate concentrations of GdmCl results in a molten globule, and while significant structure is present between 1 and ∼3 M GdmCl, particularly in the B/C barrel region, the entire ellipsoidal structure does not snap into place and is not stable until low GdmCl concentrations (<0.5 M) are reached.

How Different Are the Intermediate Ensembles and the DSE? Far-UV CD unfolding experiments reveal a gradual transition between the intermediate ensemble and the DSE (Figure 2),[7,28,31] while in DSC experiments, no heat capacity peak is observed for the intermediate to unfolded transition.[25] This behavior would be expected in the absence of an energy barrier between these conformational ensembles resulting in a continuous expansion of the α_1AT structure.[25] In spFRET experiments, continuous expansion from the intermediate to the denatured ensembles would be detected as a GdmCl-dependent change in the mean energy transfer efficiency of the intermediate peaks, as observed for the DSE (Figure 3). However, the peak centers for the intermediates are not dependent on GdmCl (Figure 3), and the peaks for the intermediate ensembles and the DSE are distinct, indicating that these are two different conformational ensembles separated by an energy barrier. In contrast to the DSC, which might not detect a small change in heat capacity, the spFRET data reveal that there is likely a small energy barrier between the intermediate and denatured state ensembles.

The DSE. Trp fluorescence studies of serpin unfolding suggest that serpins have residual secondary structure even in high concentrations of chemical denaturants, and that this residual structure helps serpins refold.[34,88] This residual structure is reported to be in the B/C barrel,[34,88] a region that is particularly stable in the native α_1AT conformation.[64] In spFRET experiments, such residual structure should reduce the R_g of the DSE. Above 5.5 M GdmCl, the R_g for α_1AT levels out around 60 Å (Figure 4), which is significantly lower than the mean R_g value of 69 Å predicted for a 394-amino acid protein based on small angle X-ray scattering data from a number of proteins but is within the 95% confidence limits.[89] It is likely that the relatively low R_g arises from residual structure because Cys232 (used in all of our labeling schemes) is located in the B/C barrel and would therefore be affected by any residual structure.

These results demonstrate the utility of using multiple labeling locations for spFRET studies to probe global protein symmetry, particularly for larger proteins. They also suggest that the ellipticity of the serpin fold, which likely facilitates the conformational changes required for protease inhibition, may also play a role in serpin folding. Interestingly, insertion of the RCL into β sheet A increases the internal symmetry of α_1AT and can result in two-state unfolding,[7] indicating that both internal and global symmetry can play a role in serpin folding.

■ ASSOCIATED CONTENT

Supporting Information

Experimental details for the spFRET and CD experiments, asphericity and shape values, fits to the CD data, and bulk fluorescence and FCS figures. This material is available free of charge via the Internet at http://pubs.acs.org.

■ AUTHOR INFORMATION

Corresponding Author

*Department of Biochemistry & Molecular Biology, Life Sciences Laboratory, Room N333, 240 Thatcher Rd., Amherst, MA 01003. E-mail: gershenson@biochem.umass.edu. Phone: (413) 545-1250. Fax: (413) 545-4020.

Present Addresses

§L.L.: Amazon.com, Inc., Irvine, CA 92618.

∥M.W.: Rush Medical College, Chicago, IL 60612.

Funding

Research reported in this publication was supported by National Science Foundation Grant MCB-0446220 and National Institute of General Medical Sciences Grant R01GM09848.

Notes

The authors declare the following competing financial interest(s): A.G. was the recipient of an Alpha-1 Foundation & Talecris Biotherapeutics Research Initiative Grant. Talecris Biotherapeutics markets α_1-antitrypsin as a pharmaceutical.

■ ACKNOWLEDGMENTS

We thank Daniel Oprian for use of his fluorescence spectrometer, J. Alejandro D'Aquino for assistance in analyzing protein structures, and Nicole Mushero for critical reading of the manuscript.

■ ABBREVIATIONS

α_1AT, α_1-antitrypsin; AF488, Alexa Fluor 488; CD, circular dichroism; DSC, differential scanning calorimetry; DSE, denatured state ensemble; FCS, fluorescence correlation spectroscopy; GdmCl, guanidinium chloride; HDXMS, hydrogen−deuterium exchange mass spectrometry; PDB, Protein Data Bank; R_g, radius of gyration; RCL, reactive center loop; spFRET, single-pair Förster resonance energy transfer; SI, stoichiometry of inhibition; TR, Texas Red.

■ REFERENCES

(1) Gettins, P. G. W. (2002) Serpin structure, mechanism, and function. *Chem. Rev. 102*, 4751−4803.

(2) Irving, J. A., Pike, R. N., Lesk, A. M., and Whisstock, J. C. (2000) Phylogeny of the serpin superfamily: Implications of patterns of amino acid conservation for structure and function. *Genome Res. 10*, 1845−1864.

(3) Dementiev, A., Dobo, J., and Gettins, P. G. W. (2006) Active site distortion is sufficient for proteinase inhibition by serpins: Structure of the covalent complex of α_1-proteinase inhibitor with porcine pancreatic elastase. *J. Biol. Chem. 281*, 3452−3457.

(4) Huntington, J. A., Read, R. J., and Carrell, R. W. (2000) Structure of a serpin-protease complex shows inhibition by deformation. *Nature 407*, 923−926.

(5) Dementiev, A., Simonovic, M., Volz, K., and Gettins, P. G. W. (2003) Canonical inhibitor-like interactions explain reactivity of α_1-

proteinase inhibitor Pittsburgh and antithrombin with proteinases. *J. Biol. Chem. 278*, 37881−37887.
(6) Ye, S., Cech, A. L., Belmares, R., Bergstrom, R. C., Tong, Y., Corey, D. R., Kanost, M. R., and Goldsmith, E. J. (2001) The structure of a Michaelis serpin-protease complex. *Nat. Struct. Biol. 8*, 979−983.
(7) Bruch, M., Weiss, V., and Engel, J. (1988) Plasma serine proteinase inhibitors (serpins) exhibit major conformational changes and a large increase in conformational stability upon cleavage at their reactive sites. *J. Biol. Chem. 263*, 16626−16630.
(8) Im, H., Seo, E. J., and Yu, M.-H. (1999) Metastability in the inhibitory mechanism of human α_1-antitrypsin. *J. Biol. Chem. 274*, 11072−11077.
(9) Seo, E. J., Im, H., Maeng, J.-S., Kim, K. E., and Yu, M.-H. (2000) Distribution of the native strain in human α_1-antitrypsin and its association with protease inhibitor function. *J. Biol. Chem. 275*, 16904−16909.
(10) Im, H., Woo, M.-S., Hwang, K. Y., and Yu, M.-H. (2002) Interactions causing the kinetic trap in serpin protein folding. *J. Biol. Chem. 277*, 46347−46354.
(11) Mottonen, J., Strand, A., Symersky, J., Sweet, R. M., Danley, D. E., Geoghegan, K. F., Gerard, R. D., and Goldsmith, E. J. (1992) Structural basis of latency in plasminogen activator inhibitor-1. *Nature 355*, 270−273.
(12) Dafforn, T. R., Mahadeva, R., Elliott, P. R., Sivasothy, P., and Lomas, D. A. (1999) A kinetic mechanism for the polymerization of α_1-antitrypsin. *J. Biol. Chem. 274*, 9548−9555.
(13) Lomas, D. A., Evans, D. L., Finch, J. T., and Carrell, R. W. (1992) The mechanism of Z α_1-antitrypsin accumulation in the liver. *Nature 357*, 605−607.
(14) Sivasothy, P., Dafforn, T. R., Gettins, P. G. W., and Lomas, D. A. (2000) Pathogenic α_1-antitrypsin polymers are formed by a reactive loop-β-sheet A linkage. *J. Biol. Chem. 275*, 33663−33668.
(15) Yamasaki, M., Li, W., Johnson, D. J. D., and Huntington, J. A. (2008) Crystal structure of a stable dimer reveals the molecular basis of serpin polymerization. *Nature 455*, 1255−1258.
(16) Yamasaki, M., Sendall, T. J., Pearce, M. C., Whisstock, J. C., and Huntington, J. A. (2011) Molecular basis of α_1-antitrypsin deficiency revealed by the structure of a domain-swapped trimer. *EMBO Rep. 12*, 1011−1017.
(17) Dima, R. I., and Thirumalai, D. (2004) Asymmetry in the shapes of folded and denatured states of proteins. *J. Phys. Chem. B 108*, 6564−6570.
(18) Stout, T. J., Graham, H., Buckley, D. I., and Matthews, D. J. (2000) Structures of active and latent PAI-1: A possible stabilizing role for chloride ions. *Biochemistry 39*, 8460−8469.
(19) Tucker, H. M., Mottonen, J., Goldsmith, E. J., and Gerard, R. D. (1995) Engineering of plasminogen activator inhibitor-1 to reduce the rate of latency transition. *Nat. Struct. Biol. 2*, 442−445.
(20) Nar, H., Bauer, M., Stassen, J.-M., Lang, D., Gils, A., and Declerck, P. J. (2000) Plasminogen activator inhibitor 1. Structure of the native serpin, comparison to its other conformers and implications for serpin inactivation. *J. Mol. Biol. 297*, 683−695.
(21) Sharp, A. M., Stein, P. E., Pannu, N. S., Carrell, R. W., Berkenpas, M. B., Ginsburg, D., Lawrence, D. A., and Read, R. J. (1999) The active conformation of plasminogen activator inhibitor 1, a target for drugs to control fibrinolysis and cell adhesion. *Structure 7*, 111−118.
(22) Jensen, J. K., and Gettins, P. G. W. (2008) High-resolution structure of the stable plasminogen activator inhibitor type-1 variant 14-1B in its proteinase-cleaved form: A new tool for detailed interaction studies and modeling. *Protein Sci. 17*, 1844−1849.
(23) Zhang, Q., Buckle, A. M., Law, R. H. P., Pearce, M. C., Cabrita, L. D., Lloyd, G. J., Irving, J. A., Smith, A. I., Ruzyla, K., Rossjohn, J., Bottomley, S. P., and Whisstock, J. C. (2007) The N terminus of the serpin, tengpin, functions to trap the metastable native state. *EMBO Rep. 8*, 658−663.
(24) Baek, J.-H., Yang, W. S., Lee, C., and Yu, M.-H. (2009) Functional unfolding of α_1-antitrypsin probed by hydrogen-deuterium exchange coupled with mass spectrometry. *Mol. Cell. Proteomics*, 1072−1081.
(25) Tsutsui, Y., and Wintrode, P. L. (2007) Cooperative unfolding of a metastable serpin to a molten globule suggests a link betwen functional and folding energy landscapes. *J. Mol. Biol. 371*, 245−255.
(26) Powell, L. M., and Pain, R. H. (1992) Effects of glycosylation on the folding and stability of human, recombinant and cleaved α_1-antitrypsin. *J. Mol. Biol. 224*, 241−252.
(27) Kim, D., and Yu, M.-H. (1996) Folding pathway of human α_1-antitrypsin: Characterization of an intermediate that is active but prone to aggregation. *Biochem. Biophys. Res. Commun. 226*, 378−384.
(28) Pearce, M. C., Rubin, H., and Bottomley, S. P. (2000) Conformational change and intermediates in the unfolding of α1-antichymotrypsin. *J. Biol. Chem. 275*, 28513−28518.
(29) Lomas, D. A., Evans, D. L., Stone, S. R., Chang, W. S., and Carrell, R. W. (1993) Effect of the Z mutation on the physical and inhibitory properties of α_1-antitrypsin. *Biochemistry 32*, 500−508.
(30) Cabrita, L. D., Whisstock, J. C., and Bottomley, S. P. (2002) Probing the role of the F-helix in serpin stability through a single tryptophan substitution. *Biochemistry 41*, 4575−4581.
(31) James, E. L., Whisstock, J. C., Gore, M. G., and Bottomley, S. P. (1999) Probing the unfolding pathway of α_1-antitrypsin. *J. Biol. Chem. 274*, 9482−9488.
(32) Krishnan, B., and Gierasch, L. M. (2011) Dynamic local unfolding in the serpin α_1-antitrypsin provides a mechanism for loop insertion and polymerization. *Nat. Struct. Mol. Biol. 18*, 222−226.
(33) Stocks, B. B., Sarkar, A., Wintrode, P. L., and Konermann, L. (2012) Early hydrophobic collapse of α_1-antitrypsin facilitates formation of a metastable state: Insights from oxidative labeling and mass spectrometry. *J. Mol. Biol. 423*, 789−799.
(34) Tew, D. J., and Bottomley, S. P. (2001) Probing the equilibrium denaturation of the serpin α_1-antitrypsin with single tryptophan mutants; evidence for structure in the urea unfolded state. *J. Mol. Biol. 313*, 1161−1169.
(35) Tsutsui, Y., Dela Cruz, R., and Wintrode, P. L. (2012) Folding mechanism of the metastable serpin α_1-antitrypsin. *Proc. Natl. Acad. Sci. U.S.A. 109*, 4467−4472.
(36) Wang, Z., Mottonen, J., and Goldsmith, E. J. (1996) Kinetically controlled folding of the serpin plasminogen activator inhibitor 1. *Biochemistry 35*, 16443−16448.
(37) Brockwell, D. J., Paci, E., Zinober, R. C., Beddard, G. S., Olmsted, P. D., Smith, D. A., Perham, R. N., and Radford, S. E. (2003) Pulling geometry defines the mechanical resistance of a β-sheet protein. *Nat. Struct. Biol. 10*, 731−737.
(38) Carrion-Vazquez, M., Li, H., Lu, H., Marszalek, P. E., Oberhauser, A. F., and Fernandez, J. M. (2003) The mechanical stability of ubiquitin is linkage dependent. *Nat. Struct. Biol. 10*, 738−743.
(39) Dietz, H., Berkemeier, F., Bertz, M., and Rief, M. (2006) Anisotropic deformation response of single protein molecules. *Proc. Natl. Acad. Sci. U.S.A. 103*, 12724−12728.
(40) Nome, R. A., Zhao, J. M., Hoff, W. D., and Scherer, N. F. (2007) Axis-dependent anisotropy in protein unfolding from integrated nonequilibrium single-molecule experiments, analysis, and simulation. *Proc. Natl. Acad. Sci. U.S.A. 104*, 20799−20804.
(41) Best, R. B., Li, B., Steward, A., Daggett, V., and Clarke, J. (2001) Can non-mechanical proteins withstand force? Stretching barnase by atomic force microscopy and molecular dynamics simulation. *Biophys. J. 81*, 2344−2356.
(42) Brockwell, D. J. (2007) Probing the mechanical stability of proteins using the atomic force microscope. *Biochem. Soc. Trans. 35*, 1564−1568.
(43) Brockwell, D. J., Beddard, G. S., Clarkson, J., Zinober, R. C., Blake, A. W., Trinick, J., Olmsted, P. D., Smith, D. A., and Radford, S. E. (2002) The effect of core destabilization on the mechanical resistance of I27. *Biophys. J. 83*, 458−472.
(44) Fowler, S. B., Best, R. B., Toca Herrera, J. L., Rutherford, T. J., Steward, A., Paci, E., Karplus, M., and Clarke, J. (2002) Mechanical unfolding of a titin Ig domain: Structure of unfolding intermediate

revealed by combining AFM, molecular dynamics simulations, NMR and protein engineering. *J. Mol. Biol. 322*, 841−849.
(45) Kuzmenkina, E. V., Heyes, C. D., and Ulrich Nienhaus, G. (2006) Single-molecule FRET study of denaturant induced unfolding of RNase H. *J. Mol. Biol. 357*, 313−324.
(46) Schuler, B., Lipman, E. A., and Eaton, W. A. (2002) Probing the free-energy surface of protein folding with single-molecule fluorescence spectroscopy. *Nature 419*, 743−747.
(47) Sherman, E., and Haran, G. (2006) Coil-globule transition in the denatured state of a small protein. *Proc. Natl. Acad. Sci. U.S.A. 103*, 11539−11543.
(48) Spyracopoulos, L. (2006) A suite of Mathematica notebooks for the analysis of protein main chain ^{15}N NMR relaxation data. *J. Biomol. NMR 36*, 215−224.
(49) Kwon, K. S., Kim, J., Shin, H. S., and Yu, M. H. (1994) Single amino acid substitutions of α_1-antitrypsin that confer enhancement in thermal stability. *J. Biol. Chem. 269*, 9627−9631.
(50) Laska, M. E. (2001) The effect of dissolved oxygen on recombinant protein degradation in *Escherichia coli*. Ph.D. Thesis, Massachusetts Institute of Technology, Cambridge, MA.
(51) Liu, L., Mushero, N., Hedstrom, L., and Gershenson, A. (2006) Conformational distributions of protease-serpin complexes: A partially translocated complex. *Biochemistry 45*, 10865−10872.
(52) Nozaki, Y. (1972) The preparation of guanidine hydrochloride. *Methods Enzymol. 26*, 43−50.
(53) Nath, U., and Udgaonkar, J. B. (1995) Perturbation of a tertiary hydrogen bond in barstar by mutagenesis of the sole His residue to Gln leads to accumulation of at least one equilibrium folding intermediate. *Biochemistry 34*, 1702−1713.
(54) Mukhopadhyay, S., Krishnan, R., Lemke, E. A., Lindquist, S., and Deniz, A. A. (2007) A natively unfolded yeast prion monomer adopts an ensemble of collapsed and rapidly fluctuating structures. *Proc. Natl. Acad. Sci. U.S.A. 104*, 2649−2654.
(55) Dahan, M., Deniz, A. A., Ha, T., Chemla, D. S., Schultz, P. G., and Weiss, S. (1999) Ratiometric measurement and identification of single diffusing molecules. *Chem. Phys. 247*, 85−106.
(56) Gopich, I. V., and Szabo, A. (2012) Theory of single-molecule FRET efficiency histograms. *Adv. Chem. Phys. 146*, 245−297.
(57) Gopich, I., and Szabo, A. (2005) Theory of photon statistics in single-molecule Förster resonance energy transfer. *J. Chem. Phys. 122*, 014707.
(58) Grosberg, A. Y., and Khokhlov, A. R. (1994) *Statistical physics of macromolecules*, AIP Press, Woodside, NY.
(59) Schuler, B., Lipman, E. A., Steinbach, P. J., Kumke, M., and Eaton, W. A. (2005) Polyproline and the "spectroscopic ruler" revisited with single-molecule fluorescence. *Proc. Natl. Acad. Sci. U.S.A. 102*, 2754−2759.
(60) Lapidus, L. J., Eaton, W. A., and Hofrichter, J. (2000) Measuring the rate of intramolecular contact formation in polypeptides. *Proc. Natl. Acad. Sci. U.S.A. 97*, 7220−7225.
(61) Elson, E. L., and Magde, D. (1974) Fluorescence correlation spectroscopy. I. Conceptual basis and theory. *Biopolymers 13*, 1−27.
(62) Thompson, N. L. (1991) Fluorescence correlation spectroscopy. In *Topics in Fluorescence Spectroscopy* (Lakowicz, J. R., Ed.) pp 337−378, Plenum Press, New York.
(63) Pu, M., Fang, X., Redfield, A. G., Gershenson, A., and Roberts, M. F. (2009) Correlation of vesicle binding and phospholipid dynamics with phospholipase C activity. *J. Biol. Chem. 284*, 16099−16107.
(64) Tsutsui, Y., Liu, L., Gershenson, A., and Wintrode, P. L. (2006) The conformational dynamics of a metastable serpin studied by hydrogen exchange and mass spectrometry. *Biochemistry 45*, 6561−6569.
(65) Lee, C., Seo, E. J., and Yu, M.-H. (2001) Role of the connectivity of secondary structure segments in the folding of α_1-antitrypsin. *Biochem. Biophys. Res. Commun. 287*, 636−641.
(66) Choi, U. B., McCann, J. J., Weninger, K. R., and Bowen, M. E. (2011) Beyond the random coil: Stochastic conformational switching in intrinsically disordered proteins. *Structure 19*, 566−576.
(67) Pirchi, M., Ziv, G., Riven, I., Cohen, S. S., Zohar, N., Barak, Y., and Haran, G. (2011) Single-molecule fluorescence spectroscopy maps the folding landscape of a large protein. *Nat. Commun. 2*, 493.
(68) Merchant, K. A., Best, R. B., Louis, J. M., Gopich, I. V., and Eaton, W. A. (2007) Characterizing the unfolded states of proteins using single-molecule FRET spectroscopy and molecular simulations. *Proc. Natl. Acad. Sci. U.S.A. 104*, 1528−1533.
(69) Hofmann, H., Soranno, A., Borgia, A., Gast, K., Nettels, D., and Schuler, B. (2012) Polymer scaling laws of unfolded and intrinsically disordered proteins quantified with single-molecule spectroscopy. *Proc. Natl. Acad. Sci. U.S.A. 109*, 16155−16160.
(70) Jamroz, M., Kolinski, A., and Kmiecik, S. (2013) CABS-flex: Server for fast simulation of protein structure fluctuations. *Nucleic Acids Res. 41*, W427−W431.
(71) Jamroz, M., Orozco, M., Kolinski, A., and Kmiecik, S. (2013) Consistent view of protein fluctuations from all-atom molecular dynamics and coarse-grained dynamics with knowledge-based force-field. *J. Chem. Theory Comput. 9*, 119−125.
(72) Gopich, I. V., and Szabo, A. (2003) Single-macromolecule fluorescence resonance energy transfer and free-energy profiles. *J. Phys. Chem. B 107*, 5058−5063.
(73) Hoffmann, A., Kane, A., Nettels, D., Hertzog, D. E., Baumgartel, P., Lengefeld, J., Reichardt, G., Horsley, D. A., Seckler, R., Bakajin, O., and Schuler, B. (2007) Mapping protein collapse with single-molecule fluorescence and kinetic synchrotron radiation circular dichroism spectroscopy. *Proc. Natl. Acad. Sci. U.S.A. 104*, 105−110.
(74) Hofmann, H., Golbik, R. P., Ott, M., Hübner, C. G., and Ulbrich-Hofmann, R. (2008) Coulomb forces control the density of the collapsed unfolded state of barstar. *J. Mol. Biol. 376*, 597−605.
(75) Schuler, B., and Eaton, W. A. (2008) Protein folding studied by single-molecule FRET. *Curr. Opin. Struct. Biol. 18*, 16−26.
(76) Ziv, G., Thirumalai, D., and Haran, G. (2009) Collapse transition in proteins. *Phys. Chem. Chem. Phys. 11*, 83−93.
(77) Haris, P. I., Chapman, D., Harrison, R. A., Smith, K. F., and Perkins, S. J. (1990) Conformational transition between native and reactive center cleaved forms of α_1-antitrypsin by Fourier transform infrared spectroscopy and small-angle neutron scattering. *Biochemistry 29*, 1377−1380.
(78) Chattopadhyay, K., Saffarian, S., Elson, E. L., and Frieden, C. (2002) Measurement of microsecond dynamic motion in the intestinal fatty acid binding protein by using fluorescence correlation spectroscopy. *Proc. Natl. Acad. Sci. U.S.A. 99*, 14171−14176.
(79) Rhoades, E., Gussakovsky, E., and Haran, G. (2003) Watching proteins fold one molecule at a time. *Proc. Natl. Acad. Sci. U.S.A. 100*, 3197−3202.
(80) Li, G., Levitus, M., Bustamante, C., and Widom, J. (2005) Rapid spontaneous accessibility of nucleosomal DNA. *Nat. Struct. Mol. Biol. 12*, 46−53.
(81) Sherman, E., Itkin, A., Kuttner, Y. Y., Rhoades, E., Amir, D., Haas, E., and Haran, G. (2008) Using fluorescence correlation spectroscopy to study conformational changes in denatured proteins. *Biophys. J. 94*, 4819−4827.
(82) Torres, T., and Levitus, M. (2007) Measuring conformational dynamics: A new FCS-FRET approach. *J. Phys. Chem. B 111*, 7392−7400.
(83) Arai, M., and Kuwajima, K. (2000) Role of the molten globule state in protein folding. *Adv. Protein Chem. 53*, 209−282.
(84) Im, H., and Yu, M. H. (2000) Role of Lys335 in the metastability and function of inhibitory serpins. *Protein Sci. 9*, 934−941.
(85) Knaupp, A. S., Keleher, S., Yang, L., Dai, W., Bottomley, S. P., and Pearce, M. C. (2013) The roles of helix I and strand 5A in the folding, function and misfolding of α_1-antitrypsin. *PLoS One 8*, e54766.
(86) Dolmer, K., and Gettins, P. G. W. (2012) How the serpin α_1-proteinase inhibitor folds. *J. Biol. Chem. 287*, 12425−12432.
(87) Onda, M., Nakatani, K., Takehara, S., Nishiyama, M., Takahashi, N., and Hirose, M. (2008) Cleaved serpin refolds into the relaxed state via a stressed conformer. *J. Biol. Chem. 283*, 17568−17578.

(88) Pearce, M. C., Cabrita, L. D., Rubin, H., Gore, M. G., and Bottomley, S. P. (2004) Identification of residual structure within denatured antichymotrypsin: Implications for serpin folding and misfolding. *Biochem. Biophys. Res. Commun. 324*, 729−735.
(89) Kohn, J. E., Millett, I. S., Jacob, J., Zagrovic, B., Dillon, T. M., Cingel, N., Dothager, R. S., Seifert, S., Thiyagarajan, P., Sosnick, T. R., Hasan, M. Z., Pande, V. S., Ruczinski, I., Doniach, S., and Plaxco, K. W. (2004) Random-coil behavior and the dimensions of chemically unfolded proteins. *Proc. Natl. Acad. Sci. U.S.A. 101*, 12491−12496.
(90) Elliott, P. R., Pei, X. Y., Dafforn, T. R., and Lomas, D. A. (2000) Topography of a 2.0 Å structure of α_1-antitrypsin reveals targets for rational drug design to prevent conformational disease. *Protein Sci. 9*, 1274−1281.
(91) Pettersen, E. F., Goddard, T. D., Huang, C. C., Couch, G. S., Greenblatt, D. M., Meng, E. C., and Ferrin, T. E. (2004) UCSF Chimera: A visualization system for exploratory research and analysis. *J. Comput. Chem. 25*, 1605−1612.